International Journal of Bifurcation and Chaos

Structurally unstable synchronization and border-collision bifurcations in the two-coupled Izhikevich neuron model

Yuu Miino
Graduate School of Education, Naruto University of Education, 748, Takashima, Naruto, 772-8502, Tokushima, Japan
miino.yuu@gmail.com

Tetsushi Ueta
Center for Administration of Information Technology, Tokushima University, 2-1, Minamijosanjima, Tokushima, 770-8506, Tokushima, Japan
ueta@tokushima-u.ac.jp

Received (to be inserted by publisher)

This study investigates a structurally unstable synchronization phenomenon observed in the two-coupled Izhikevich neuron model. As the result of varying the system parameter in the region of parameter space close to where the unstable synchronization is observed, we find significant changes in the stability of its periodic motion. We derive a discrete-time dynamical system that is equivalent to the original model and reveal that the unstable synchronization in the continuous-time dynamical system is equivalent to border-collision bifurcations in the corresponding discrete-time system. Furthermore, we propose an objective function that can be used to obtain the parameter set at which the border-collision bifurcation occurs. The proposed objective function is numerically differentiable and can be solved using Newton's method. We numerically generate a bifurcation diagram in the parameter plane, including the border-collision bifurcation sets. In the diagram, the border-collision bifurcation sets show a novel bifurcation structure that resembles the 'strike-slip fault' observed in geology. This structure implies that, before and after the border-collision bifurcation occurs, the stability of the periodic point discontinuously changes in some cases but maintains in other cases. In addition, we demonstrate that a border-collision bifurcation sets successively branch at distinct points. This behavior results in a tree-like structure being observed in the border-collision bifurcation diagram; we refer to this structure as a *border-collision bifurcation tree*. We observe that a periodic point disappears at the border-collision bifurcation in the discrete-time dynamical system and is simultaneously replaced by another periodic point; this phenomenon corresponds to a change in the firing order in the continuous-time dynamical system.

Keywords: two-coupled Izhikevich neuron model, structurally unstable synchronization, border-collision bifurcation

1. Introduction

Neural networks have been widely used in fields including artificial intelligence, machine learning, and pattern recognition [Sapounaki & Kakarountas, 2019; Heidarpur *et al.*, 2019; Vazquez, 2010]. The mathematical model refferred to as the neuron model has been widely used to construct neural networks. In

1907, Lapicque designed the first neuron model [Lapicque, 1907]. The integrate-and-fire model is so named because it includes integration and voltage resetting; the model is still used in researche today [Kang *et al.*, 2021; Rozenberg *et al.*, 2019]. Hodgkin and Huxley proposed a model to describe how action potentials in neurons occur and propagate; this model is called the Hodgkin-Huxley model [Hodgkin & Huxley, 1952]. This model exhibits a variety of nonlinear phenomena as a result of the nonlinearity in the model; these phenomena include oscillations, bifurcations, and chaos [Feudel *et al.*, 2000]. Izhikevich proposed another model, which included a set of nonlinear differential equations and one discontinuous jumping [Izhikevich, 2003]. The Izhikevich model is now more widely used [Wang *et al.*, 2022; Tolba *et al.*, 2019] as it is numerically efficient and expresses almost all firing patterns. In the coupled Izhikevich neuron model, one can observe the synchronous firing of the neurons [Vivekanandhan *et al.*, 2022; Shafiei *et al.*, 2019]. This represents a well-known phenomenon that also occurs in the human brain; this phenomenon plays an important role in neuron communication.

From the standpoint of nonlinear dynamics, the discontinuous jumping that is present in the model is an attractive feature. When we evaluate the qualitative property of the model, it is essential to take into account the effect of the jump. Tamura *et al.* focused on this jump and proposed results based on local stability and local bifurcation analyses of an Izhikevich neuron model [Tamura *et al.*, 2009]. They used a hybrid system approach, as proposed in Ref. [Kousaka *et al.*, 1999], to analyze the model and to classify the solutions according to their topological properties. Later, Ito *et al.* broadened the applicability of the method proposed by Tamura *et al.* to include the two-coupled Izhikevich neuron model [Ito *et al.*, 2010]. The work of Ito *et al.* is significant as it can be used to analyze large coupled systems, such as neural networks. We note here that in Ref. [Ito *et al.*, 2010] there is no consideration of the synchronous firing of neurons.

Many studies on border-collision bifurcation are present in the literature; these studies are primarily related to mechanics and electronics [Nusse *et al.*, 1994; Simpson, 2016; Banerjee & Grebogi, 1999]. This variety of a bifurcation occurs for a periodic point in discrete-time hybrid dynamical systems that include a threshold or a border in the state space. The typical scenario for the bifurcation is that a periodic point moves as a result of the manipulation of the parameters describing the system, arrives at a threshold or border, and suddenly alternates its stability or disappears. A similar phenomenon may occur in discretized systems, such as the Poincaré map, and even in continuous-time hybrid dynamical systems. The appropriate analysis method of border-collision bifurcations is dependent on the threshould definition. If the target system is comprised of linear systems and switches via an external periodic clock input, one can analytically solve the bifurcation problem, as suggested by Kousaka *et al.* [Kousaka *et al.*, 2002]. If the threshold periodically moves, the method proposed by Ma *et al.* [Ma *et al.*, 2004] works well. Yamashita and Torikai observed border-collision bifurcations in a qualitatively similar system to the Izhikevich neuron model [Yamashita & Torikai, 2012]. However, studies investigating the bifurcations in the original Izhikevich model have not yet been undertaken.

Our previous study [Miino & Ueta, 2016] observed the synchronous firing phenomenon in the two-coupled Izhikevich neuron model but did not establish that the phenomenon was equivalent to a bifurcation in the context of nonlinear dynamics. It is notable that the observed firing pattern is structurally unstable, whereas commonly observed patterns, like spike synchronization or complete synchronization, are typically structurally stable (against pertubations in the system parameters). However, the study did not investigate the structural stability and presented only preliminary discussions related to the bifurcation. This study names the observed firing pattern "structurally unstable synchronization" and extends the previous discussions related to the bifurcations within the same model using the Poincaré map approach. The Poincaré map is by definition qualitatively equivalent to the original model and is a powerful tool in the analysis of the periodic motions within the model. This study reveals that the phenomenon is essentially equivalent to the border-collision bifurcation. Furthermore, we develop a novel method to obtain the parameter set for which the border-collision bifurcation occurs, i.e., the parameter set that induces an unstable synchronization. We measure the local stability of the periodic motion by considering the Jacobian matrix of the Poincaré map. Consequently, we reveal the effect of the bifurcations on the local stability. We observe that the bifurcation diagram includes local and border-collision bifurcations, and we summarize the characteristics of structurally unstable synchronizations.

This paper has the following structure. In Sec. 2, we describe the systems that are analyzed here. We introduce the Izhikevich neuron model, its counterpart two-coupled model, and the structurally unstable synchronization phenomenon; we also describe the equations that underpin the model, firing boundaries, and the firing phenomenon of a single neuron. We define the three-dimensional Poincaré map obtained from the four-dimensional original model by discretizing its trajectory at the time at which a neuron fires. The periodic point observed in the Poincaré map is topologically equivalent to the periodic motion in the coupled Izhikevich model. We quantify the local stability using the Jacobian matrix for the discretized system. We outline the method first proposed in Ref. [Kousaka *et al.*, 1999] and use it to compute the relevant Jacobian matrix. We also explain the method that we use to locate the local bifurcation sets to investigate the existence of periodic points. In the last subsection of Sec. 2, we describe the border-collision bifurcation observed in the Poincaré map. We mathematically demonstrate the equivalence between the unstable synchronization and the border-collision bifurcation. In Sec. 3, we propose a numerical method that can be used to find the unstable synchronization parameter, i.e., a method that can be used to find the border-collision bifurcation parameter. We formulate an objective function representing the criteria for the unstable synchronization to occur and solve it via numerical optimization. We suggest a calculation method based on Newton's method to obtain the partial derivatives of the objective function. In Sec. 4, we discuss the results of the numerical work undertaken here. The results presented in this work include a two-parameter bifurcation diagram, a one-parameter diagram, a collection of the attractors, a transition of the eigenvalues, and a change in the eigenvectors. Based on the obtained results, we summarize the characteristics of the border-collision bifurcation, i.e., the structurally unstable synchronization phenomenon. We conclude and summarize the study in Sec. 5.

2. Model

2.1. *The Izhikevich neuron model and the corresponding coupled model*

The Izhikevich neuron model [Izhikevich, 2003] is a system of two ordinary differential equations:

$$\frac{dv}{dt} = 0.04v^2 + 5v + 140 - u + I, \quad \frac{du}{dt} = a(bv - u), \tag{1}$$

and a map representing the auxiliary after-spike resetting,

$$(v, u) \mapsto (c, u + d), \quad \text{if} \quad v \geq 30, \tag{2}$$

where v is the membrane potential of a neuron, u is the recovery variable, I is the synaptic currents or injected DC-currents, a is the timescale of u, b is the sensitivity of u to v, c is the after-spike reset value of v, and d is the after-spike reset value of u.

Connecting two neurons via a gap junction, we obtain the two-coupled Izhikevich neuron model [Ito *et al.*, 2010] described by

$$\begin{aligned}
\frac{dv_\alpha}{dt} &= 0.04v_\alpha^2 + 5v_\alpha + 140 - u_\alpha + I_\alpha + \delta(v_\alpha - v_\beta),\\
\frac{du_\alpha}{dt} &= a_\alpha(b_\alpha v_\alpha - u_\alpha),\\
\frac{dv_\beta}{dt} &= 0.04v_\beta^2 + 5v_\beta + 140 - u_\beta + I_\beta + \delta(v_\beta - v_\alpha),\\
\frac{du_\beta}{dt} &= a_\beta(b_\beta v_\beta - u_\beta),
\end{aligned} \tag{3}$$

and

$$\begin{aligned}
(v_\alpha, u_\alpha, v_\beta, u_\beta) &\mapsto (c_\alpha, u_\alpha + d_\alpha, v_\beta, u_\beta), \quad \text{if} \quad v_\alpha \geq 30,\\
(v_\alpha, u_\alpha, v_\beta, u_\beta) &\mapsto (v_\alpha, u_\alpha, c_\beta, u_\beta + d_\beta), \quad \text{if} \quad v_\beta \geq 30,
\end{aligned} \tag{4}$$

where the α and β used as subscripts identify the neurons and δ is the coupling coefficient. When manipulating the system parameters, the coupled model is seen to exhibit a rich variety of trajectories, including periodic motions with various periods, and chaotic motions.

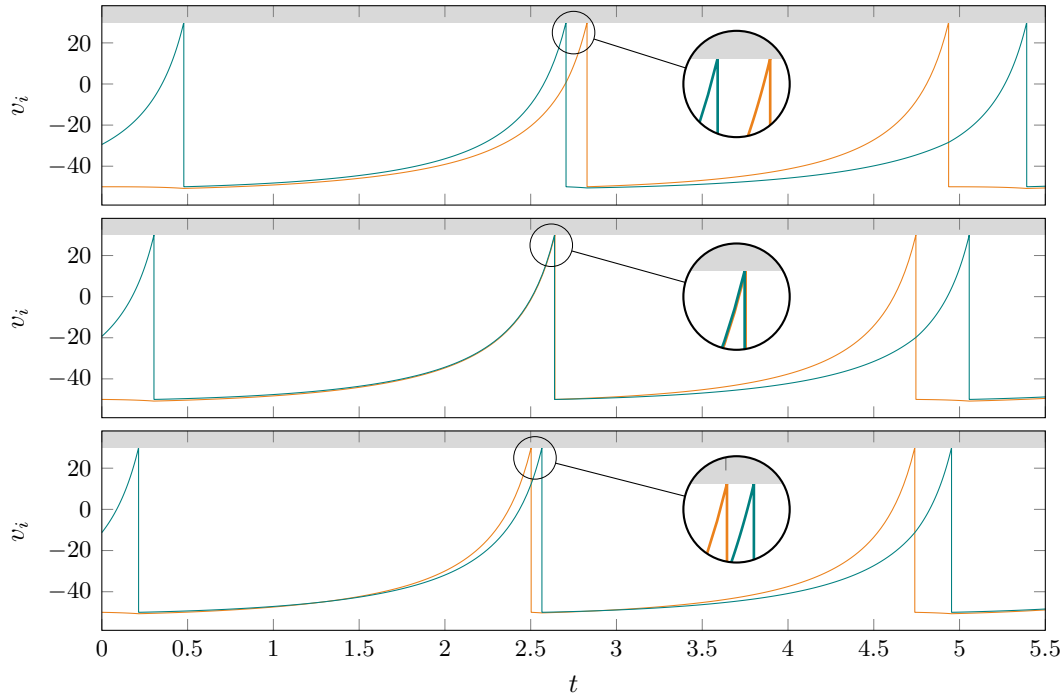

Fig. 1. Example of a periodic motion near the structurally unstable synchronization with $\delta = -0.1$ and (top) $a_\alpha = 0.22$, (middle) $a_\alpha = 0.243153$, and (bottom) $a_\alpha = 0.245$. Other parameters values are fixed, as given in Eq. (29). The orange and green curves show the trajectories of v_α and v_β, respectively. The middle figure shows the case of a structurally unstable synchronization. The gray shaded area denotes the region for which $v_i > 30$.

Synchronous firing is the phenomenon in which the firing of multiple neurons is coincident, i.e., $v_\alpha = v_\beta = 30$. In the two-coupled case, it can be seen that the phenomenon can be structurally unstable to parameter perturbations. We refer to this phenomenon as the *structurally unstable synchronization* case. Figure 1 shows an example of a structurally unstable synchronization observed in the periodic motion of the model. In the top figure (for $a_\alpha = 0.22$), at around $t = 0.27$, neuron β fires prior to neuron α. By increasing the value of a_α, it can be seen that neuron β fires at the same time as neuron α, as shown in the middle figure ($a_\alpha = 0.243153$). By increasing further, the order of the firing reverses, as shown in the bottom figure. We show here that in this observed change in the order of firing of the neurons, the stability of the periodic motion is drasrtically changed (see Sec. 4).

2.2. *Mathematical definitions*

In the vector form, the system described by (3) is written in

$$\frac{d\boldsymbol{v}}{dt} = \boldsymbol{f}_\lambda(\boldsymbol{v}), \quad \boldsymbol{v} \in M, \tag{5}$$

where $\boldsymbol{v} = (v_\alpha, u_\alpha, v_\beta, u_\beta)$ is a state variable vector, $\boldsymbol{f}_\lambda : M \to \mathbb{R}^4$ is a vector-valued function representing the right-hand side of Eq. (3), λ represents a controllable parameter of the system (3), i.e., $\lambda \in \{a_i, c_i, I_i\} \cup \{\delta\}$ for $i \in \{\alpha, \beta\}$, and M is a manifold defined by

$$M = \left\{ \boldsymbol{v} \in \mathbb{R}^4 \mid v_\alpha \leq 30 \text{ and } v_\beta \leq 30 \right\}. \tag{6}$$

The maps given in Eq. (4) are described by

$$\begin{aligned} F_\alpha &: \Pi_{\alpha^-} \to \Pi_{\alpha^+}; \quad \boldsymbol{v} \mapsto \boldsymbol{v} + \boldsymbol{c}_\alpha, \\ F_\beta &: \Pi_{\beta^-} \to \Pi_{\beta^+}; \quad \boldsymbol{v} \mapsto \boldsymbol{v} + \boldsymbol{c}_\beta, \end{aligned} \tag{7}$$

where

$$\begin{aligned}
\Pi_{\alpha^-} &= \left\{\boldsymbol{v} \in M \;\middle|\; q_\alpha(\boldsymbol{v}) = v_\alpha - 30 = 0\right\}, \quad \Pi_{\alpha^+} = \left\{\boldsymbol{v} \in M \;\middle|\; v_\alpha - c_\alpha = 0\right\}, \\
\Pi_{\beta^-} &= \left\{\boldsymbol{v} \in M \;\middle|\; q_\beta(\boldsymbol{v}) = v_\beta - 30 = 0\right\}, \quad \Pi_{\beta^+} = \left\{\boldsymbol{v} \in M \;\middle|\; v_\beta - c_\beta = 0\right\}, \\
\boldsymbol{c}_\alpha &= \begin{bmatrix} -30 + c_\alpha \\ d_\alpha \\ 0 \\ 0 \end{bmatrix}, \qquad \boldsymbol{c}_\beta = \begin{bmatrix} 0 \\ 0 \\ -30 + c_\beta \\ d_\beta \end{bmatrix}.
\end{aligned} \tag{8}$$

2.3. *Poincaré map*

Let $\boldsymbol{\varphi}_\lambda$ be the solution trajectory of the system described by Eq. (5) together with an initial state $\boldsymbol{v}_0$ at $t = 0$, such that $\boldsymbol{v}(t) = \boldsymbol{\varphi}_\lambda(\boldsymbol{v}_0, t)$, and let τ_k be the time interval between the $(k-1)$-th firing of a neuron and the k-th firing of the same or a different neuron in the system. Then, the trajectory starting from $\boldsymbol{v}_0 \in \Pi_{\alpha^+}$ and returning to Π_{α^+} as a result of neuron β firing N times can be decomposed into the following maps:

$$\begin{aligned}
T_0 &: \Pi_{\alpha^+} \to \Pi_{\beta^-} \to \Pi_{\beta^+}; && \boldsymbol{v}_0 \mapsto \boldsymbol{\varphi}_\lambda(\boldsymbol{v}_0, \tau_1) \mapsto \boldsymbol{v}_1 = F_\beta(\boldsymbol{\varphi}_\lambda(\boldsymbol{v}_0, \tau_1)), \\
T_1 &: \Pi_{\beta^+} \to \Pi_{\beta^-} \to \Pi_{\beta^+}; && \boldsymbol{v}_1 \mapsto \boldsymbol{\varphi}_\lambda(\boldsymbol{v}_1, \tau_2) \mapsto \boldsymbol{v}_2 = F_\beta(\boldsymbol{\varphi}_\lambda(\boldsymbol{v}_1, \tau_2)), \\
&\vdots \\
T_{N-1} &: \Pi_{\beta^+} \to \Pi_{\beta^-} \to \Pi_{\beta^+}; && \boldsymbol{v}_{N-1} \mapsto \boldsymbol{\varphi}_\lambda(\boldsymbol{v}_{N-1}, \tau_N) \\
&&& \qquad \mapsto \boldsymbol{v}_N = F_\beta(\boldsymbol{\varphi}_\lambda(\boldsymbol{v}_{N-1}, \tau_N)), \\
T_N &: \Pi_{\beta^+} \to \Pi_{\alpha^-} \to \Pi_{\alpha^+}; && \boldsymbol{v}_N \mapsto \boldsymbol{\varphi}_\lambda(\boldsymbol{v}_N, \tau_{N+1}) \\
&&& \qquad \mapsto F_\alpha(\boldsymbol{\varphi}_\lambda(\boldsymbol{v}_N, \tau_{N+1})).
\end{aligned} \tag{9}$$

In this study, we construct the Poincaré map of the coupled Izhikevich neuron model by composing the maps T_k

$$T_{[N]} : \Pi_{\alpha^+} \to \Pi_{\alpha^+}; \quad \boldsymbol{v}_0 \mapsto T_{[N]}(\boldsymbol{v}) = T_N \circ T_{N-1} \circ \cdots \circ T_0(\boldsymbol{v}_0). \tag{10}$$

We note that for the case of $N = 0$, we have

$$T_{[0]} : \Pi_{\alpha^+} \to \Pi_{\alpha^-} \to \Pi_{\alpha^+}; \quad \boldsymbol{v}_0 \mapsto \boldsymbol{\varphi}_\lambda(\boldsymbol{v}_0, \tau_1) \mapsto \boldsymbol{v}_1 = F_\alpha(\boldsymbol{\varphi}_\lambda(\boldsymbol{v}_0, \tau_1)). \tag{11}$$

Since T includes a trivial element that is tangent to Π_{α^+} (which is parallel to the direction of v_α-axis), we can degenerate T into another equivalent map, $U_{[N]}$:

$$U_{[N]} : \Pi_0 \to \Pi_0; \quad \boldsymbol{x}_0 \mapsto p^{-1} \circ T_{[N]} \circ p(\boldsymbol{x}_0), \tag{12}$$

where $\boldsymbol{x} = (u_\alpha, v_\beta, u_\beta)$, $\Pi_0 = \left\{\boldsymbol{x} \in \mathbb{R}^3 \;\middle|\; v_\beta \leq 30\right\}$, and

$$\begin{aligned}
p &: \Pi_0 \to \Pi_{\alpha^+}; && \boldsymbol{x}_0 = (u_\alpha, v_\beta, u_\beta) \mapsto \boldsymbol{v}_0 = (c_\alpha, u_\alpha, v_\beta, u_\beta), \\
p^{-1} &: \Pi_{\alpha^+} \to \Pi_0; && \boldsymbol{v} = (c_\alpha, u_\alpha, v_\beta, u_\beta) \mapsto \boldsymbol{x} = (u_\alpha, v_\beta, u_\beta).
\end{aligned} \tag{13}$$

We can then consider the discrete-time dynamical system

$$\boldsymbol{x}_{n+1} = U_{[N_n]}(\boldsymbol{x}_n), \quad n \in \mathbb{Z}^+, \tag{14}$$

where $\mathbb{Z}^+$ is the set of non-negative integers, rather than the original continuous-time dynamical system to solve the stability problem of the periodic motion. We note that the value of N_n is dependent on $\boldsymbol{x}_n$ but can only be obtained after the evaluation of $\boldsymbol{x}_{n+1}$ as N_n is the number of firings that occur prior to the state $\boldsymbol{x}_{n+1}$ being realized.

Figure 2 summarizes the mathematical definitions used here as well as the Poincaré map of the model illustrated using an example solution trajectory. In the figure, we use the initial state $\boldsymbol{x}_0 = (-2.17, -29.43, -4.41) \in \Pi_0$. The map p maps $\boldsymbol{x}_0$ to $\boldsymbol{v}_0 = (-50, -2.17, -29.43, -4.41) \in \Pi_{\alpha^+}$, which is the initial state of the original time-continuous model. Solving the original model, we find that

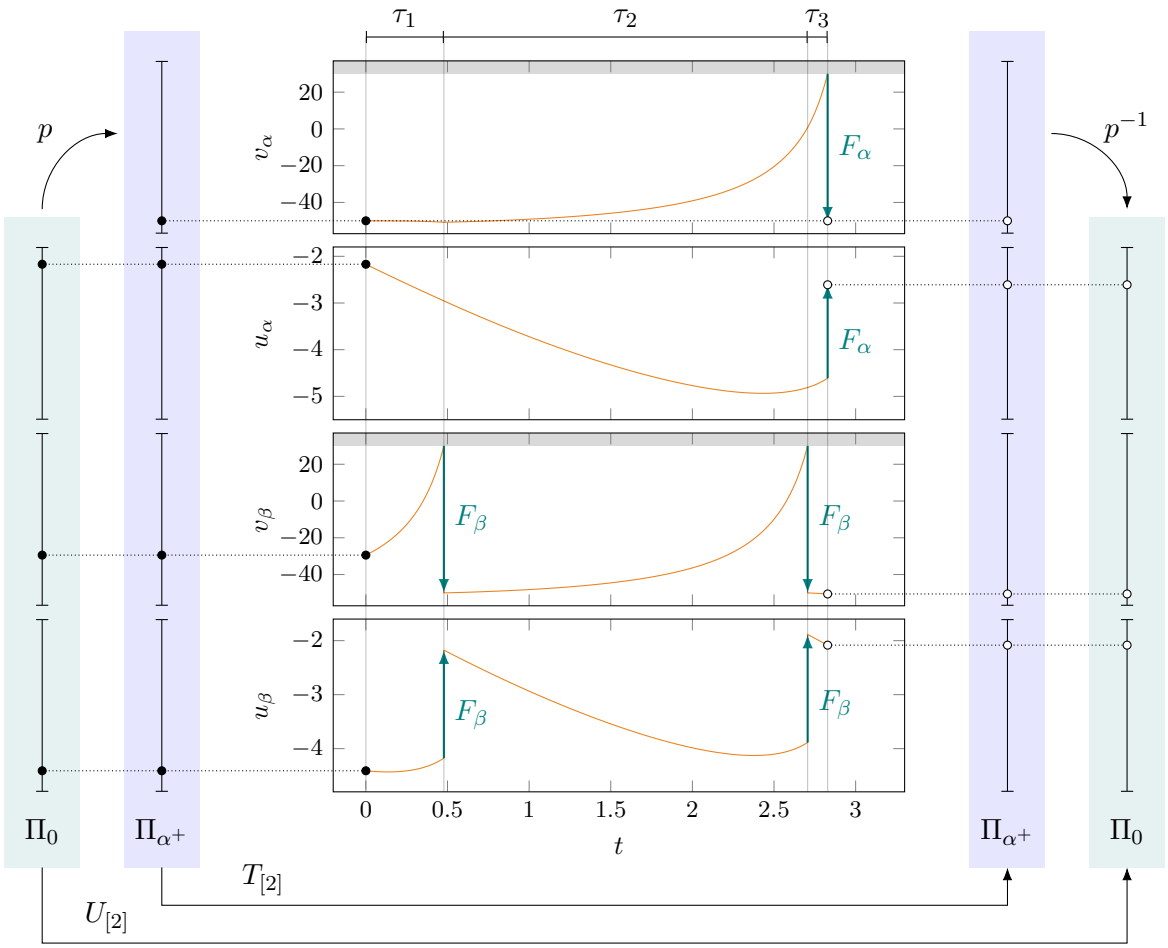

Fig. 2. Schematic of the definitions considered here and the Poincaré map. The filled points represent the initial state, $\boldsymbol{x}_0 = (-2.17, -29.43, -4.41)$ in Π_0 and $\boldsymbol{v}_0 = p(\boldsymbol{x}_0) = (-50, -2.17, -29.43, -4.41)$ in $\Pi_{\alpha+}$; the unfilled points represent the next states of the discrete-time system, $(-50, -2.61, -50.57, -2.08)$ in $\Pi_{\alpha+}$ and $\boldsymbol{x}_1 = p^{-1}(-50, -2.61, -50.57, -2.08) = (-2.61, -50.57, -2.08)$ in Π_0.

$(-50, -2.61, -50.57, -2.08) \in \Pi_{\alpha+}$ at $t \approx 2.83$, which is the time at which φ_λ first reaches $\Pi_{\alpha-}$. In the time interval $t \in [0, 2.83]$, neuron β fires twice, i.e., $N_0 = 2$. Thus, we can describe the Poincaré map in $\Pi_{\alpha+}$ as $T_{[2]}(-50, -2.17, -29.43, -4.41) = (-50, -2.61, -50.57, -2.08)$. Since we have the same value of v_α in the manifold $\Pi_{\alpha+}$, we can reduce the dimension of the state by using p^{-1}: $p^{-1}(-50, -2.61, -50.57, -2.08) = (-2.61, -50.57, -2.08)$. Hence, we can describe the next state, $\boldsymbol{x}_1$, of the degenerate Poincaré map in Π_0 as $\boldsymbol{x}_1 = U_{[2]}(\boldsymbol{x}_0) = (-2.61, -50.57, -2.08)$.

2.4. *Periodic points and their local stability*

A point $\boldsymbol{x}^*$ that satisfies

$$U_{[N_\ell - 1]} \circ U_{[N_{\ell-2}]} \circ \cdots \circ U_{[N_0]}(\boldsymbol{x}^*) - \boldsymbol{x}^* = \boldsymbol{0}, \tag{15}$$

is an ℓ-periodic point of U, which corresponds to a periodic motion in the original model. The local stability of $\boldsymbol{x}^*$ can be evaluated by considering the Jacobian matrix of $U^\ell = U_{[N_\ell - 1]} \circ U_{[N_{\ell-2}]} \circ \cdots \circ U_{[N_0]}$ at $\boldsymbol{x}^*$. An ℓ-periodic point $\boldsymbol{x}^*$ is asymptotically stable if all the eigenvalues of the matrix are within the unit circle on the complex plane; $\boldsymbol{x}^*$ is unstable if some eigenvalue(s) is(are) outside of this unit circle.

From Eq. (12) and using the chain rule of differentiation, we can obtain the following expression as

the Jacobian matrix,

$$\left.\frac{\partial U^\ell}{\partial \boldsymbol{x}_0}\right|_{\boldsymbol{x}_0=\boldsymbol{x}^*} = \frac{\partial p^{-1}}{\partial \boldsymbol{v}} \left(\prod_{n=0}^{\ell-1} \left.\frac{\partial T_{[N_{\ell-1-n}]}}{\partial \boldsymbol{v}_0}\right|_{\boldsymbol{v}_0=\boldsymbol{v}^*_{\ell-1-n}} \right) \Bigg|_{\boldsymbol{v}_0=\boldsymbol{v}^*} \frac{\partial p}{\partial \boldsymbol{x}_0} \tag{16}$$

where $\boldsymbol{v}^* = p(\boldsymbol{x}^*)$ and

$$\frac{\partial p^{-1}}{\partial \boldsymbol{v}} = \begin{bmatrix} 0 & 1 & 0 & 0 \\ 0 & 0 & 1 & 0 \\ 0 & 0 & 0 & 1 \end{bmatrix}, \qquad \frac{\partial p}{\partial \boldsymbol{x}_0} = \begin{bmatrix} 0 & 0 & 0 \\ 1 & 0 & 0 \\ 0 & 1 & 0 \\ 0 & 0 & 1 \end{bmatrix}. \tag{17}$$

From Eq. (10), it can be seen that the Jacobian matrix of $T_{[N_n]}$ at $\boldsymbol{v}^*_n$ is described by

$$\left.\frac{\partial T_{[N_n]}}{\partial \boldsymbol{v}_0}\right|_{\boldsymbol{v}_0=\boldsymbol{v}^*_n} = \left(\prod_{k=0}^{N} \frac{\partial T_{N_{N-k}}}{\partial \boldsymbol{v}_{N-k}} \right) \Bigg|_{\boldsymbol{v}_0=\boldsymbol{v}^*_n}. \tag{18}$$

From Eq. (9), it can be seen that the Jacobian matrices of each local map T_k at $\boldsymbol{v}_k$ are given by

$$\begin{aligned} \frac{\partial T_k}{\partial \boldsymbol{v}_k} &= \frac{\partial F_\beta}{\partial \boldsymbol{v}} \left[\left.\frac{\partial \boldsymbol{\varphi}_\lambda}{\partial \boldsymbol{v}_0}(\tau_k)\right|_{\boldsymbol{v}_0=\boldsymbol{v}_k} + \boldsymbol{f}_\lambda(\boldsymbol{v}_{k+1}) \frac{\partial \tau_{k+1}}{\partial \boldsymbol{v}_k} \right] \\ &= \left[I - \frac{1}{\frac{dq_\beta}{d\boldsymbol{v}} \boldsymbol{f}_\lambda(\boldsymbol{v}_{k+1})} \boldsymbol{f}_\lambda(\boldsymbol{v}_{k+1}) \frac{dq_\beta}{d\boldsymbol{v}} \right] \left.\frac{\partial \boldsymbol{\varphi}_\lambda}{\partial \boldsymbol{v}_0}(\tau_k)\right|_{\boldsymbol{v}_0=\boldsymbol{v}_k} \end{aligned}, \tag{19}$$

for $N \geq 1$ and $0 \leq k < N$, where I is the 4×4 identity matrix. The Jacobian matrices of the first and last local maps are given by

$$\frac{\partial T_k}{\partial \boldsymbol{v}_k} = \left[I - \frac{1}{\frac{dq_\alpha}{d\boldsymbol{v}} \boldsymbol{f}_\lambda(\boldsymbol{v}_{k+1})} \boldsymbol{f}_\lambda(\boldsymbol{v}_{k+1}) \frac{dq_\alpha}{d\boldsymbol{v}} \right] \left.\frac{\partial \boldsymbol{\varphi}_\lambda}{\partial \boldsymbol{v}_0}(\tau_k)\right|_{\boldsymbol{v}_0=\boldsymbol{v}_k}, \tag{20}$$

for $N = 0$ and $k = N$, respectively. The derivation of Eqs. (19) and (20) is provided in Ref. [Kousaka *et al.*, 1999]. The partial derivative of $\boldsymbol{\varphi}_\lambda$ with respect to $\boldsymbol{v}_0$ can be obtained as the solution of the following differential equation:

$$\frac{d}{dt}\frac{\partial \boldsymbol{\varphi}_\lambda}{\partial \boldsymbol{v}_0} = \frac{d\boldsymbol{f}_\lambda}{d\boldsymbol{v}}(\boldsymbol{\varphi}_\lambda) \frac{\partial \boldsymbol{\varphi}_\lambda}{\partial \boldsymbol{v}_0}, \quad \frac{\partial \boldsymbol{\varphi}_\lambda}{\partial \boldsymbol{v}_0}(0) = \frac{\partial \boldsymbol{v}_0}{\partial \boldsymbol{v}_0} = I. \tag{21}$$

2.5. *Local bifurcations*

By controlling the system parameter λ, the stability of an ℓ-periodic point can be changed from stable to unstable, and vice versa. This change in stability is referred to as a local bifurcation. A local bifurcation causes a significant change in the vector field of U, including the appearance or disappearance of periodic points. Since the eigenvalues of the Jacobian matrix determine the stability, we can classify the local bifurcations by considering the expression,

$$\det \left(\left.\frac{\partial U^\ell}{\partial \boldsymbol{x}_0}\right|_{\boldsymbol{x}_0=\boldsymbol{x}^*} - e^{j\theta} I \right) = 0, \tag{22}$$

where $j = \sqrt{-1}$, and θ indicates the argument of the eigenvalue with a magnitude equal to one. Three types of local bifurcations can be observed: a tangent bifurcation (for $\theta = 0$), a period-doubling bifurcation ($\theta = \pi$), and a Neimark-Sacker bifurcation otherwise.

Numerical methods including Newton's method can be used to solve Eqs. (15) and (22) simultaneously. In the case where the derivatives of U^ℓ with respect to the parameter λ are required, we can derive them using the method proposed in Ref. [Ito *et al.*, 2010].

2.6. *Border-collision bifurcation*

The discrete-time dynamical system described in Eq. (14) is defined in Π_0, which is the manifold with the boundary

$$\partial\Pi_0 = \left\{ \boldsymbol{x} \in \Pi_0 \;\middle|\; v_\beta = 30 \right\}. \tag{23}$$

Considering an ℓ-periodic point $\boldsymbol{x}^*$ near the boundary and manipulating some system parameters, we translate $\boldsymbol{x}^*$ onto $\partial\Pi_0$. Around such a parameter setting, we can observe the appearance/disappearance of $\boldsymbol{x}^*$ by perturbing the controlling parameter. In the discrete-time discontinuous dynamical systems, this sudden appearance or disappearance of $\boldsymbol{x}^*$ represents a border-collision bifurcation of $\boldsymbol{x}^*$.

In order to analyze border-collision bifurcations, it is useful to consider a ℓ-periodic point $\boldsymbol{x}_0^*$ of U and another ℓ-periodic point $\boldsymbol{x}_1^*$ that satisfies the following condition:

$$U_{[N_0]}(\boldsymbol{x}_0^*) = \boldsymbol{x}_1^*; \tag{24}$$

we assume $\boldsymbol{x}_1^*$ is the point that appears or disappears as a result of the border-collision bifurcation. Hence, we describe the criterion for a border-collision bifurcation of the ℓ-periodic point $\boldsymbol{x}_1^*$ as

$$U_{[N_0]}(\boldsymbol{x}_0^*) = \boldsymbol{x}_1^* \in \partial\Pi_0. \tag{25}$$

We can rewrite Eq. (25) as

$$\begin{aligned}
& U_{[N_0]}(\boldsymbol{x}_0^*) \in \partial\Pi_0, \\
\Rightarrow\quad & p^{-1} \circ T_{[N_0]} \circ p(\boldsymbol{x}_0^*) \in \partial\Pi_0, \\
\Rightarrow\quad & p \circ p^{-1} \circ T_{[N_0]}(\boldsymbol{v}_0^*) \in p[\partial\Pi_0] = \left\{ \boldsymbol{v} \in M \;\middle|\; v_\alpha = c_\alpha \text{ and } v_\beta = 30 \right\} \\
\Rightarrow\quad & \boldsymbol{v}_1^* \in \left\{ \boldsymbol{v} \in M \;\middle|\; v_\alpha = c_\beta \text{ and } v_\beta = 30 \right\}, \\
\Rightarrow\quad & F_\alpha^{-1}(\boldsymbol{v}_1^*) \in F_\alpha^{-1}\left[p[\partial\Pi_0]\right] = \left\{ \boldsymbol{v} \in M \;\middle|\; v_\alpha = 30 \text{ and } v_\beta = 30 \right\} \\
& \qquad\qquad = \Pi_{\alpha^-} \cap \Pi_{\beta^-},
\end{aligned}$$

where $F_\alpha^{-1} : \Pi_{\alpha^+} \to \Pi_{\alpha^-}; \boldsymbol{v} \mapsto \boldsymbol{v} - \boldsymbol{c}_\alpha$. The last equation given above represents the criterion for the synchronous firing phenomenon to occur. Thus, the border-collision bifurcation of an ℓ-periodic point in the discrete-time dynamical system (described by Eq. (14)) is identical to the synchronous firing phenomenon of a periodic motion in the original continuous-time model. We note that the equivalence is not always present in the case of a smooth system showing synchronous motions as the border-collision requires a border within the domain of the map, like the firing border in the Izhikevich neuron model.

3. Obtaining a parameter set that corresponds to a synchronous firing event

Let t_n be the time at which a neuron fires for the n-th time, synchronous firing is defined by

$$t_N - t_{N+1} = 0. \tag{26}$$

Since t_{N+1} is the time at which neuron α first fires and t_N is the time at which neuron β fires for the N-th time, they satisfy

$$\lim_{t \to t_{N+1}^-} q_\alpha(\boldsymbol{v}(t)) = 0 \quad \text{and} \quad \lim_{t \to t_N^-} q_\beta(\boldsymbol{v}(t)) = 0, \tag{27}$$

where the concept of limits is necessary because the left-sided limit of $\boldsymbol{v}(t)$ indicates the state before firing whereas the right-sided limit represents the state after firing. The state $\boldsymbol{v} \in M$ at the time t depends on the initial value $\boldsymbol{x}_0 \in \Pi_0$ and the system parameters, i.e., t_{N+1} and t_N are implicit functions of $(\boldsymbol{x}_0, \lambda)$, as defined by Eq. (27). Hence, we can rewrite the condition given in Eq. (26) as

$$t_N(\boldsymbol{x}_0, \lambda) - t_{N+1}(\boldsymbol{x}_0, \lambda) = 0. \tag{28}$$

As in the case of the local bifurcation sets, numerical methods including Newton's method can be used to solve Eqs. (15) and (28) simultaneously; this can be done using the left-hand side of the two expressions as an objective function. When the derivatives of t_n are necessary, the method presented in Ref. [Miino

et al., 2015] can be used to derive them. This method adds a new state variable that is equivalent to time, t. It then calculates the required derivatives with respect to an initial state or a system parameter by composing the Jacobian matrices of the local maps. Alternatively, the following recurrence relation can be used to calculate the derivatives

$$\frac{\partial t_n}{\partial \boldsymbol{x}_0} = \frac{\partial}{\partial \boldsymbol{x}_0}(t_{n-1}+\tau_n) = \frac{\partial t_{n-1}}{\partial \boldsymbol{x}_0} + \frac{\partial \tau_n}{\partial \boldsymbol{x}_{n-1}}\frac{\partial \boldsymbol{x}_{n-1}}{\partial \boldsymbol{x}_0}, \qquad \text{with} \quad \frac{\partial t_1}{\partial \boldsymbol{x}_0} = \frac{\partial \tau_1}{\partial \boldsymbol{x}_0},$$
$$\frac{\partial t_n}{\partial \lambda} = \frac{\partial}{\partial \lambda}(t_{n-1}+\tau_n) = \frac{\partial t_{n-1}}{\partial \lambda} + \frac{\partial \tau_n}{\partial \boldsymbol{x}_{n-1}}\frac{\partial \boldsymbol{x}_{n-1}}{\partial \lambda} + \frac{\partial \tau_n}{\partial \lambda}, \quad \text{with} \quad \frac{\partial t_1}{\partial \lambda} = \frac{\partial \tau_1}{\partial \lambda},$$

for $2 \le n \le N+1$. The derivatives of $\boldsymbol{x}_{n-1}$ and τ_n can be obtained by calculating the Jacobian matrix of the Poincaré map. Reference [Ito *et al.*, 2010] provides more details regarding their derivations.

4. Numerical results

In the numerical work undertaken here, we considered the following parameters to have fixed values:

$$a_\beta = 0.2, b_i = 0.2, c_i = -50, d_i = 2, I_i = 10, \tag{29}$$

for $i \in \{\alpha, \beta\}$, and used (a_α, δ) as the bifurcation parameter. For $a_\alpha = 0.2$, the system described in Eq. (5) is equivariant [Chossat & Lauterbach, 2000] with respect to the cyclic group $Z_2 = \langle\gamma\rangle$, where $\gamma : (v_\alpha, u_\alpha, v_\beta, u_\beta) \mapsto (v_\beta, u_\beta, v_\alpha, u_\alpha)$. Considering two neurons with identical initial states and $a_\alpha = 0.2$, we observe complete synchronization within the system, i.e., neurons α and β are identical. On the other hand, if $\boldsymbol{x}^*$ is an ℓ-periodic point with $a_\alpha = 0.2$, $\gamma(\boldsymbol{v}^*)$ is also an ℓ-periodic point regardless of whether $\boldsymbol{v}^* = \gamma(\boldsymbol{v}^*)$ or $\boldsymbol{v}^* \neq \gamma(\boldsymbol{v}^*)$.

Using Newton's method, we can then numerically obtain the local and border-collision bifurcation points by solving Eqs. (15) and (22) for the local bifurcations and Eqs. (15) and (28) for the border-collision bifurcations. Here, we set the tolerance in the method to be 1×10^{-7}. We also use the parameter continuation method to compute the bifurcation curves from the obtained bifurcation points.

4.1. *Bifurcation diagram in the parameter plane*

Figure 3 shows the numerically obtained results. Considering the tangent bifurcation sets G^1 and I^1 and I^2, it can be seen that there is a symmetry with respect to the line $a_\alpha = 0.2$. The line represents the border-collision bifurcation set BC^1 of a 1-periodic point. It is expected that $a_\alpha = 0.2$ corresponds to BC^1 as the original model is an equivariant dynamical system for $a_\alpha = 0.2$. In other words, BC^1 is the border-collision bifurcation set of $\boldsymbol{v}^*$ that satisfies $\boldsymbol{v}^* = \gamma(\boldsymbol{v}^*)$. Far from the line $a_\alpha = 0.2$, at $a_\alpha = 0.4$ for example, a period-doubling cascade of I^1, I^2, and further I^ℓ can be observed. This represents a typical scenario in which chaotic motion can be observed.

Considering the border-collision bifurcations BC^2 in Fig. 3, we observe the mechanism by which the attractor is affected. Figure 4 shows the one-parameter bifurcation diagram for the same parameter interval used in Fig. 3. To generate this figure, a_α was decreased from 0.31 to 0.14 in 2,000 steps, 1,000 counts of Poincaré map (Eq. (12)) were calculated for each parameter, and the last 150 v_β values were plotted. Let us confirm the change in the attractor that occurs as the parameter decrease by observing Fig. 5. Prior to the tangent bifurcation occurring, the model shows aperiodic motion in the region close to $a_\alpha = 0.3$. After the bifurcation occurs, a 1-periodic trajectory can be observed (around $a_\alpha = 0.28$). This presents a stable attractor that maintains its stability until the period-doubling bifurcation I^1 occurs. Afterward, around $a_\alpha = 0.25$, the 1-periodic trajectory becomes unstable, and a new stable 2-periodic trajectory appears. The 2-periodic trajectory includes two 2-periodic points: $\boldsymbol{x}^*$, and $U_{[1]}(\boldsymbol{x}^*)$. As shown in the trajectory, $\boldsymbol{x}^*$ is very close to the line $v_\beta = 30$, which is the boundary Π_{β^-}. The point $\boldsymbol{x}^*$ approaches the line as a_α decreases and finally contacts the boundary at the line labeled BC^2. At that point, $\boldsymbol{x}^*$ undergoes a border-collision bifurcation and disappears. We note that the periodic point $U_{[1]}(\boldsymbol{x}^*)$ also disappears at this time. Simultaneously, a new 2-periodic point $\overline{\boldsymbol{x}^*}$ appears close to Π_{β^+} as shown in the trajectory depicted at $a_\alpha = 0.245$; equivalently, a point $U_{[0]}(\overline{\boldsymbol{x}^*})$ also appears. One may hypothesize that $\boldsymbol{x}^*$ and $\overline{\boldsymbol{x}^*}$

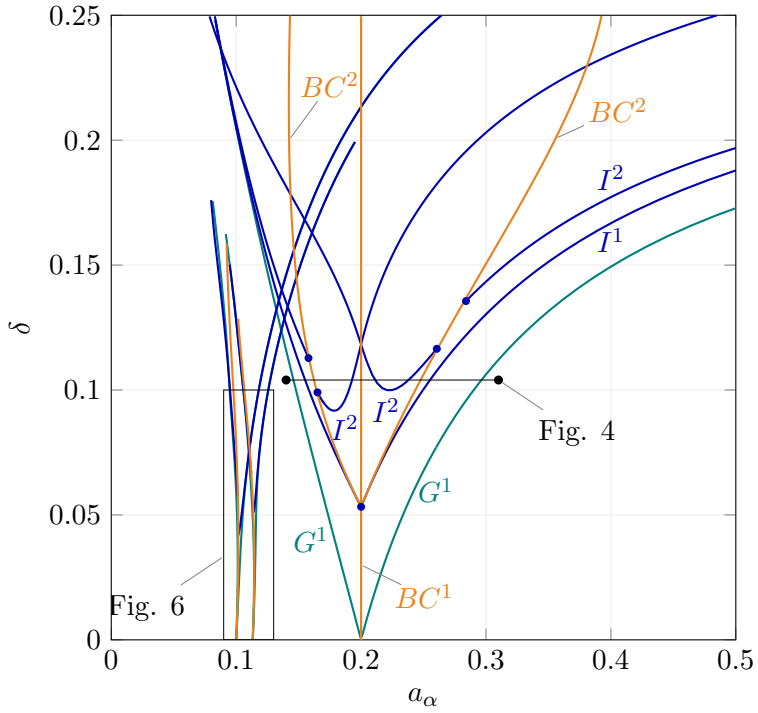

Fig. 3. Bifurcation diagram of the two-coupled Izhikevich neuron model with $a_\alpha \in [0, 0.6]$ and $\delta \in [0, 0.25]$. The green curves labeled G^ℓ represent tangent bifurcation sets, the blue curves labeled I^ℓ are period-doubling bifurcation sets, and the orange curves labeled BC^ℓ represent border-collision bifurcation sets. The superscript ℓ denotes the period ℓ of the periodic point. The region within the rectangle in the bottom left of the plot is shown in more detail in Fig. 6.

are equal and the point $\boldsymbol{x}^*$ jumps to $\overline{\boldsymbol{x}^*}$. This could be considered more plausible as the equivalent pair of $\boldsymbol{x}^*$, $U_{[1]}(\boldsymbol{x}^*)$, seems to smoothly evolve into $U_{[0]}(\overline{\boldsymbol{x}^*})$ around BC^2. Due to this smoothness, it might be hypothesized that points on either side of BC^2 are equal. However, in terms of topological conjugacy, they are distinct periodic points: $\boldsymbol{x}^*$ indeed disappears, and a distinct 2-periodic point simultaneously emerges. We will investigate the behavior of the system at BC^2 in the next subsection. At $a_\alpha = 0.235$, via the period-doubling bifurcation I^2, the 2-periodic point becomes unstable, and another stable 4-periodic trajectory

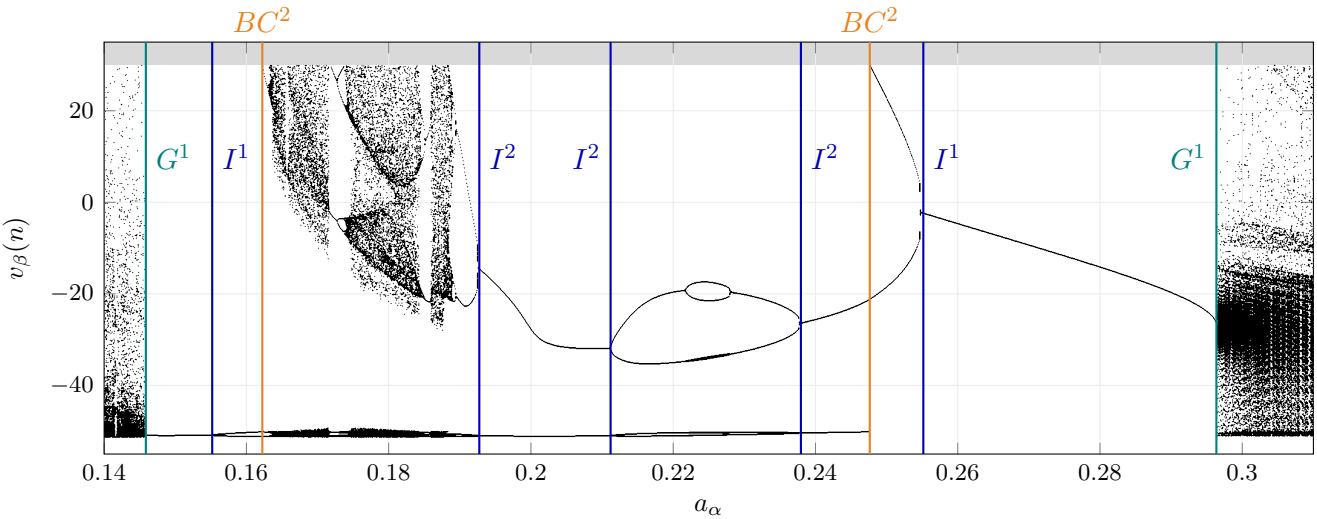

Fig. 4. One-parameter bifurcation diagram of the Poincaré map given in Eq. (12) for $a_\alpha \in [0.14, 0.31]$ and $\delta = 0.104$. $v_\beta(n)$ represents the value of v_β at $\boldsymbol{x}_n$. The vertical lines indicate the bifurcation parameters obtained in Fig. 3.

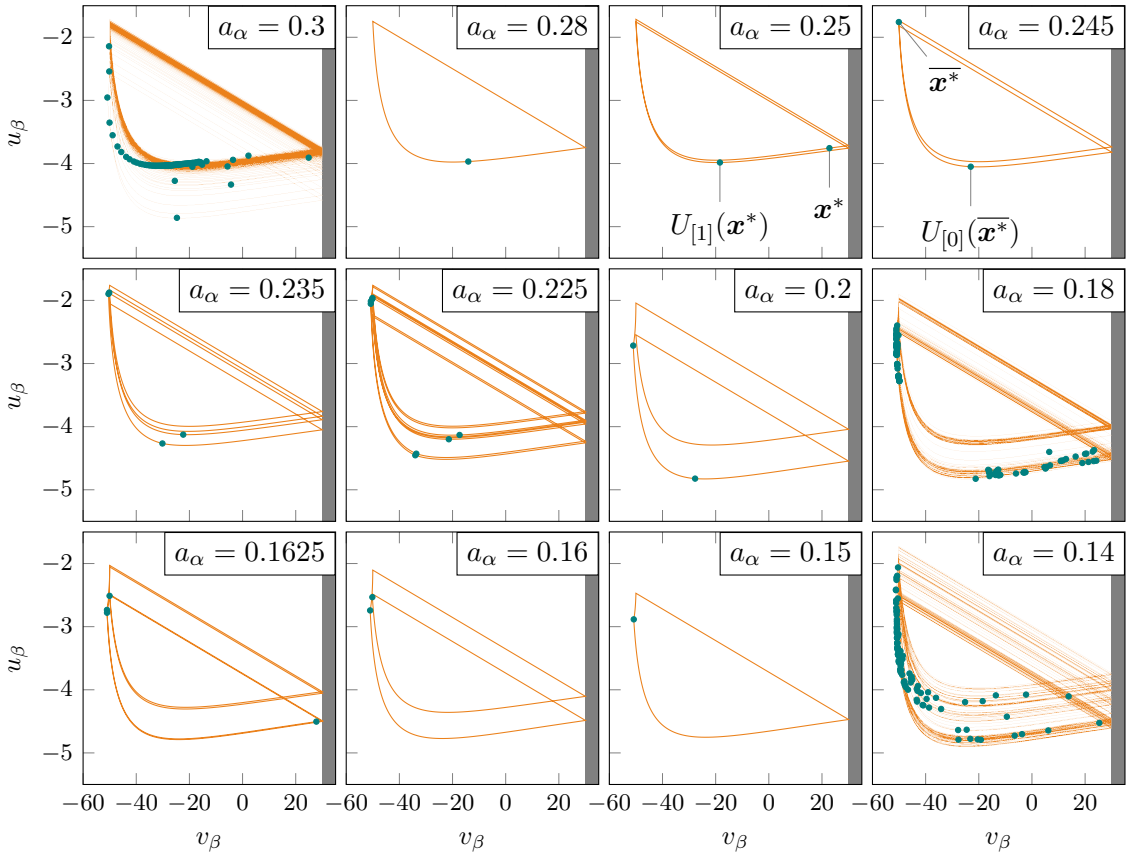

Fig. 5. A collection of the attractors in the (v_β, u_β)-plane of the coupled Izhikevich neuron model (Eq. (5)) with $\delta = 0.104$. The points in each trajectory represent the corresponding Poincaré map in the same plane.

appears. No evidence of chaotic motion around $a_\alpha = 0.235$ is observed as the period-doubling cascade stops by I^4. Further decreasing a_α to 0.2, the stable 4-periodic trajectory disappears, and a 2-periodic point again becomes stable via the reverse process of I^2. We note that the 2-periodic points observed at $a_\alpha = 0.2$ are topologically equivalent to the 2-periodic points at $a_\alpha = 0.245$. Furthermore, by decreasing a_α until 0.18, a chaotic attractor caused by a period-doubling cascade can be observed. The attractor is present until around $a_\alpha = 0.164$ and evolves into the periodic motion via a period-doubling cascade in reverse. For $a_\alpha = 0.1625$, we observe the 4-periodic points; however, this behavior disappears at the line labeled BC^2; simultaneously, a new 2-periodic trajectory emerges like the trajectory observed around $a_\alpha = 0.16$. The observed phenomenon is quite similar to the period-doubling bifurcation, however, it is not equivalent as the transition of the eigenvalues of the point is not smooth, as shown in Fig. 9. The 2-periodic points then disappear via the period-doubling bifurcation I^2, and a stable 1-periodic point appears as the attractor. We note that the 1-periodic point at $a_\alpha = 0.15$ is not topologically equivalent to the one observed at $a_\alpha = 0.28$ as it undergoes the border-collision bifurcation BC^1 at $a_\alpha = 0.2$. Finally, the 1-periodic point disappears via the tangent bifurcation G^1, and the attractor turns into an aperiodic motion at around $a_\alpha = 0.14$.

Here, we focus on the region of the parameter space that is shown in Fig. 6. In this region, the cusp structures of tangent bifurcation sets G^3 and G^4 can be observed. Inside both cusps, the border-collision bifurcation sets BC^3 and BC^4 exist along with the tangent bifurcation sets. One can also observe the period-doubling bifurcation sets I^3 and I^4 departing from the border-collision bifurcations. Despite the two branches of I^3 both being 3-periodic points, they are observed to depart from different points on BC^3. This implies the existence of different 3-periodic points on the left- and right-hand sides of BC^3. Otherwise, the two branches of I^3 would be smoothly connected. The set BC^4 also separates I^4 into two components in a similar manner; the sets BC^2 in Fig. 3 are also similar. In other words, the border-collision bifurcation sets cut the period-doubling bifurcation sets into two parts and shifts them in different directions. This

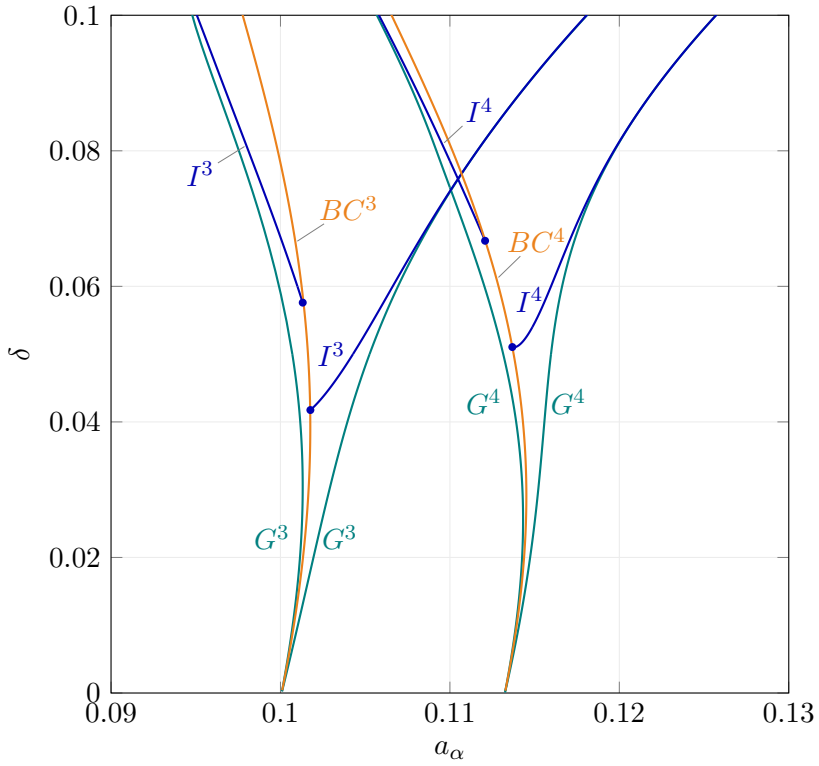

Fig. 6. A detailed view of the region within Fig. 3 with $a_\alpha \in [0.09, 0.13]$ and $\delta \in [0, 0.1]$.

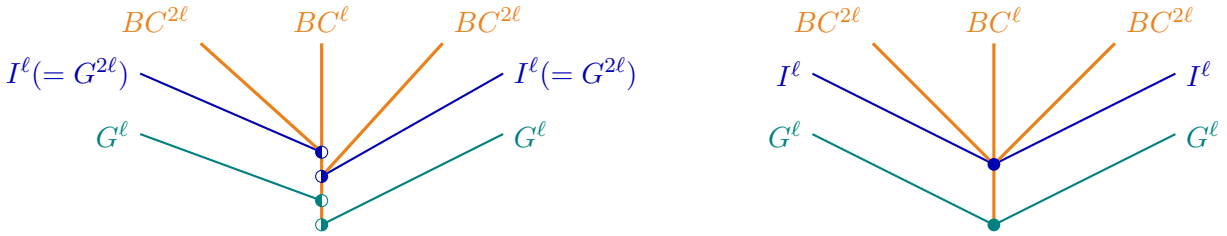

(a) General BC^ℓ. (b) BC^ℓ with complete synchronization.

Fig. 7. Schematics of the bifurcation structures around the border-collision bifurcations in a parameter plane. (a) The general case ($\ell > 1$ in the numerical work), which shows a 'strike-slip fault' structure cutting and shifting the period-doubling bifurcation sets. The half-filled circles indicate the local bifurcation points in the border-collision bifurcation sets; the direction of the circles shows the location of the focusing periodic point seen from BC^ℓ. (b) Case of BC^ℓ with complete synchronization ($\ell = 1$ in the numerical work). The filled circles represent the local bifurcation points in BC^ℓ.

novel structure of the bifurcation set resembles a 'strike-slip fault' observed in geology. Figure 7 (a) shows a schematic of the strike-slip fault structure of a period-doubling cascade for an ℓ-periodic point. Due to the structure, the attractor sometime maintains its form through the border collision, and the other case changes its form to another attractor, which is periodic or aperiodic. We note here that the numerical computation of the local bifurcations was stopped where it arrived at the border-collision bifurcation sets. This implies that the border-collision bifurcation erases the periodic point, and the numerical method thus misses the target point. The observed behavior cannot be explained without considering border collisions. Figure 8 shows the border-collision bifurcation diagram of the two-coupled Izhikevich neuron model. The sets of BC^2 can be seen to branch from a single point in BC^1, which is with complete synchronization, whereas the sets of BC^4 branch from distinct points in BC^2. We hypothesis that this branching will continue as long as the period-doubling bifurcation cascade continues. We refer to the tree structure of the border-collision bifurcation sets as the *border-collision bifurcation tree (BC tree)*. We note that any other

kind of border-collision bifurcations can occur without branching from the BC tree if it is independent of local bifurcations.

4.2. *Border-collision bifurcations and related periodic points*

Let us consider the border-collision bifurcation of 2-periodic points shown in Fig. 9. Around $a_\alpha = 0.162$, we observe two 2-periodic points: the one labeled $\boldsymbol{x}_0^*$ is unstable, and the point labeled $\overline{\boldsymbol{x}_0^*}$ is stable. On manipulating a_α from 0.164 to the point of BC^2, the unstable point approaches $\Pi_{\beta-}$, i.e., v_β^* approaches $v_\beta = 30$. As a result of the border-collision bifurcation, $\boldsymbol{x}_0^*$ suddenly disappears. However, the pair of $\boldsymbol{x}_0^*$, which is denoted $\boldsymbol{x}_1^*$ and depicted by the violet curves in the figure, seems not to disappear as a result of BC^2 as the coordinate of the point continuously transitions across BC^2. This phenomenon is highly unusual as $\boldsymbol{x}_1^*$ should disappear simultaneously with $\boldsymbol{x}_0^*$ disappearing. To understand this phenomenon, we evaluate the eigenvectors of the pair, as shown in Fig. 10. For $a_\alpha = 0.162$, one of the eigenvectors of the pair point is a real vector and the others are complex vectors. In the case of the complex vectors, we have drawn the eigenspace spanned by the vectors rather than showing the vectors. The difference to the point spirally converges in the eigenspace around the periodic point. We can thus classify the point as a spiral sink based on the behavior of its corresponding eigenvalues. By contrast, with $a_\alpha = 0.164$, all the eigenvalues are real vectors. By observing the corresponding eigenvalues, we can classify the point as a saddle. A spiral sink and a saddle are topologically distinct, even though their coordinates are precisely the same. In other words, remarkably, the periodic points before and after the border-collision bifurcation are topologically different, despite them sharing a single coordinate in the state space. Hence, we conclude that $\boldsymbol{x}_1^*$ disappears simultaneously with $\boldsymbol{x}_0^*$; however, another periodic point, $\overline{\boldsymbol{x}_1^*}$, appears simultaneously and is (by coincidence) located at the coordinate of $\boldsymbol{x}_1^*$.

In the case of complete synchronization, the coupling term always becomes zero since $v_\alpha(t) = v_\beta(t)$ [Elkaranshawy *et al.*, 2021]. This is represented by the case of $a_\alpha = 0.2$ in this study. In such a case, the coupled system reduces to that comprising uncoupled single neuron systems sharing some parameter. The synchronous motions in the single systems independently (but identically) change as a result of the shared parameter changing. In other words, such synchronous motions are structurally stable unless the single systems are structurally unstable. Thus, the period-doubling bifurcation sets on both sides of the

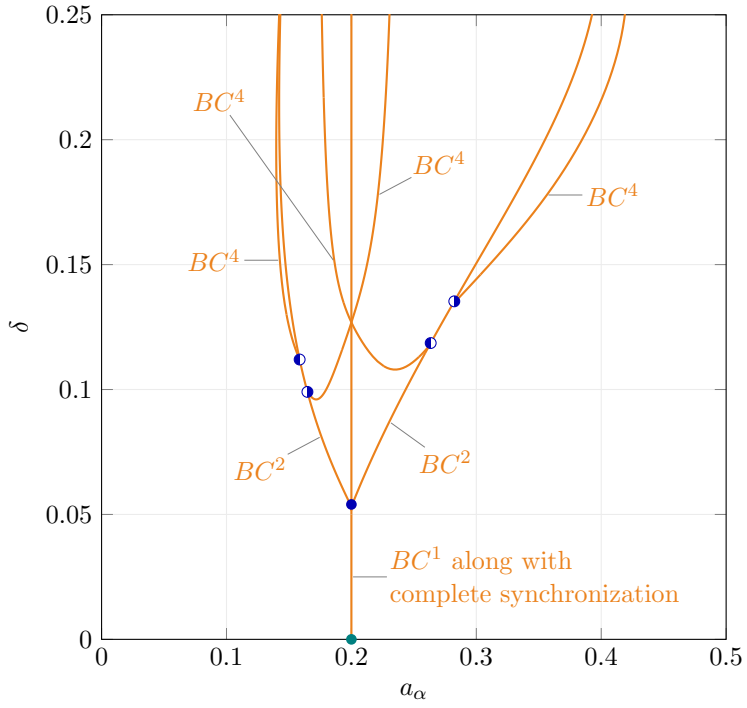

Fig. 8. Bifurcation diagram for BC^ℓ with $\ell = 1, 2$, and 4.

line $a_\alpha = 0.2$ share a single point on the line, as shown by BC^1 in Fig. 3 and generalized in Fig. 7 (b). Based on the above considerations, the authors conclude that complete synchronization in the Izhikevich model is a particular case of border-collision bifurcations and is structurally stable because the parameter moves across the bifurcation curve.

On the left- and right-hand sides of the border-collision bifurcation BC^2 near $a_\alpha = 0.248$, two 2-periodic points that are both stable and have similar trajectories can be observed. In such a case, their eigenvalues are different, as shown in the top right window of Fig. 9; there is a similar difference in their eigenvectors. We note that they represent the same type of periodic points, i.e., stable spiral sinks; nevertheless, topologically, they are distinct periodic points.

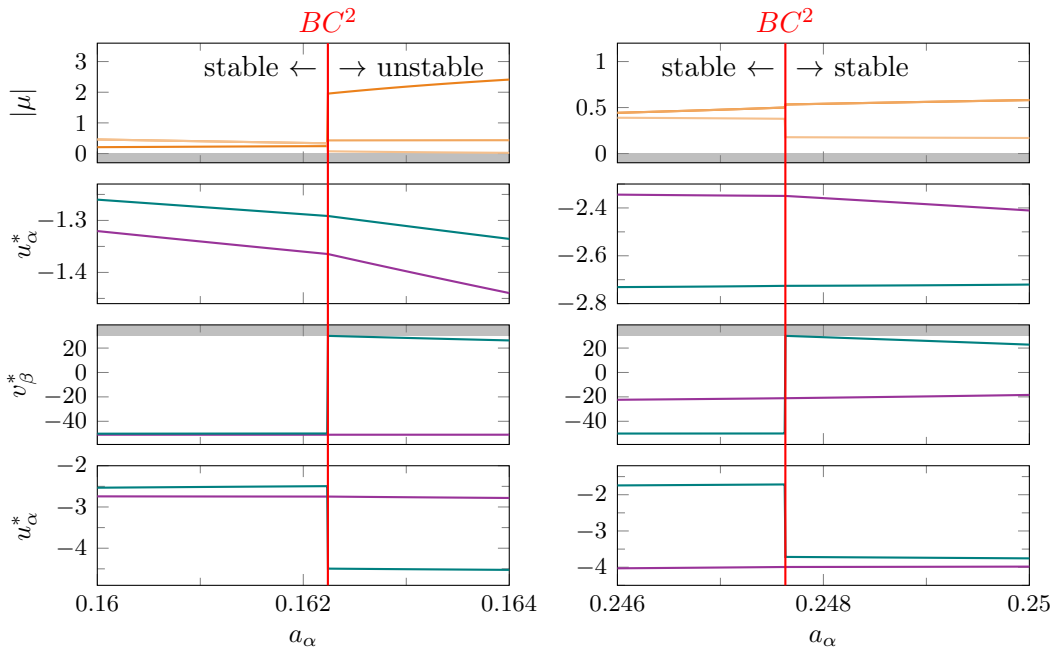

Fig. 9. Transitions of 2-periodic points and their eigenvalues μ (their absolute values are shown) around the border-collision bifurcation parameters with $\delta = 0.104$. The left figure shows that the BC^2 causes a change in the stability of the point; the right figure shows the case in which there are no changes in the stability. In the trajectory figures, the green curves indicate $\boldsymbol{x}_0^*$ and $\overline{\boldsymbol{x}_0^*}$ and the violet curves show the other periodic points $\boldsymbol{x}_1^* = U_{[2]}(\boldsymbol{x}^*)$ and $\overline{\boldsymbol{x}_1^*} = U_{[1]}\left(\overline{\boldsymbol{x}^*}\right)$, which are the equivalent periodic points to $\boldsymbol{x}_0^*$ and $\overline{\boldsymbol{x}_0^*}$, respectively.

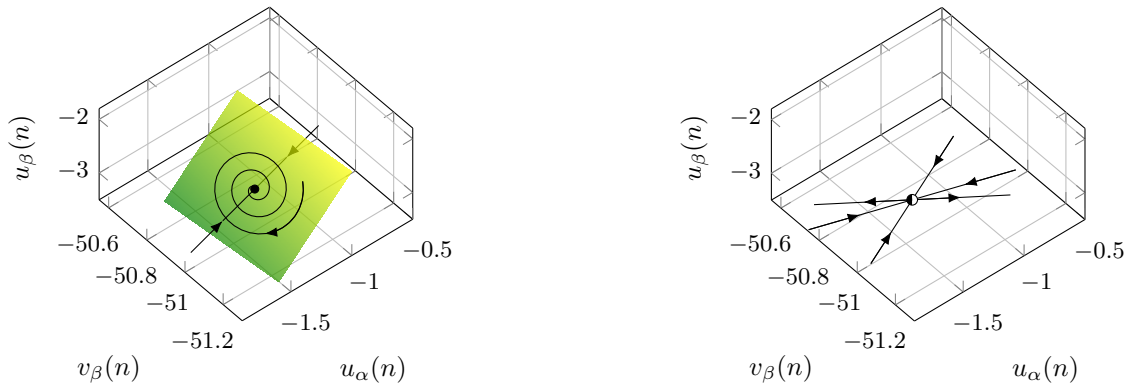

(a) $\overline{\boldsymbol{x}_1^*}$ with $a_\alpha = 0.162$.

(b) $\boldsymbol{x}_1^*$ with $a_\alpha = 0.164$.

Fig. 10. Comparison of the eigenvectors of the 2-periodic point of U before and after the border-collision bifurcation. In the case of $a_\alpha = 0.162$, we have drawn only one eigenvector and depicted a single eigenspace for the other eigenvalues as the other eigenvectors are complex vectors.

Here, we briefly derive the topological difference in the periodic points by considering an example from the region close to $a_\alpha = 0.162$. Suppose again that $\boldsymbol{x}_0^*$ and $\boldsymbol{x}_1^*$ are unstable 2-periodic points of U for $a_\alpha = 0.1625$, and $\overline{\boldsymbol{x}_0^*}$ and $\overline{\boldsymbol{x}_1^*}$ are the stable 2-periodic points for $a_\alpha = 0.162$. As defined in Sec. 2.3, U^2 for the periodic points $\boldsymbol{x}_1^*$ and $\overline{\boldsymbol{x}_1^*}$ can be decomposed into

$$\begin{aligned} U^2(\boldsymbol{x}_1^*) = U_{[2]} \circ U_{[0]}(\boldsymbol{x}_1^*) \quad &= \left(p^{-1} \circ (T_2 \circ T_1 \circ T_0) \circ T_0\right)(\boldsymbol{v}_1^*) \\ &= \left(p^{-1} \circ \left(T_\beta^\alpha \circ T_\beta^\beta \circ T_\alpha^\beta\right) \circ T_\alpha^\alpha\right)(\boldsymbol{v}_1^*), \\ U^2\left(\overline{\boldsymbol{x}_1^*}\right) = U_{[1]} \circ U_{[1]}\left(\overline{\boldsymbol{x}_1^*}\right) \quad &= \left(p^{-1} \circ (T_1 \circ T_0) \circ (T_1 \circ T_0)\right)\left(\overline{\boldsymbol{v}_1^*}\right) \\ &= \left(p^{-1} \circ \left(T_\beta^\alpha \circ T_\alpha^\beta\right) \circ \left(T_\beta^\alpha \circ T_\alpha^\beta\right)\right)\left(\overline{\boldsymbol{v}_1^*}\right), \end{aligned}$$

where $\boldsymbol{v}_1^* = p(\boldsymbol{x}_1^*)$, $\overline{\boldsymbol{v}_1^*} = p(\overline{\boldsymbol{x}_1^*})$, and $T_{i_{\text{from}}}^{i_{\text{to}}}$ denotes the map from $\Pi_{i_{\text{from}}^+} \to \Pi_{i_{\text{to}}^+}$. We note that the result of the numerical integration of the trajectory determines the firing count N. In the right-hand sides of both expressions, the maps labeled T_α^β and T_β^α are present, while the maps labeled T_α^α and T_β^β are not present in the second equation. Consequently, they are distinct maps. It is thus natural that $\boldsymbol{x}_1^*$ forms a spiral sink, while $\overline{\boldsymbol{x}_1^*}$ forms a saddle. It is generally impossible to define a homeomorphism between a spiral and a saddle. In other words, the mappings are topologically not conjugate near $\boldsymbol{x}_1^*$ or $\overline{\boldsymbol{x}_1^*}$. Furthermore, the Jacobian matrices of U^2 at $\boldsymbol{x}_1^*$ and $\overline{\boldsymbol{x}_1^*}$ are described as

$$\begin{aligned} \left.\frac{\partial U^2}{\partial \boldsymbol{x}_0}\right|_{\boldsymbol{x}_0=\boldsymbol{x}_1^*} &= \frac{\partial p^{-1}}{\partial \boldsymbol{v}} \left(\frac{\partial T_\beta^\alpha}{\partial \boldsymbol{v}_2}\frac{\partial T_\beta^\beta}{\partial \boldsymbol{v}_1}\frac{\partial T_\alpha^\beta}{\partial \boldsymbol{v}_0}\right)\Bigg|_{\boldsymbol{v}_0=\boldsymbol{v}_0^*} \left(\frac{\partial T_\alpha^\alpha}{\partial \boldsymbol{v}_0}\right)\Bigg|_{\boldsymbol{v}_0=\boldsymbol{v}_1^*} \frac{\partial p}{\partial \boldsymbol{x}_0}, \\ \left.\frac{\partial U^2}{\partial \boldsymbol{x}_0}\right|_{\boldsymbol{x}_0=\overline{\boldsymbol{x}_1^*}} &= \frac{\partial p^{-1}}{\partial \boldsymbol{v}} \left(\frac{\partial T_\beta^\alpha}{\partial \boldsymbol{v}_1}\frac{\partial T_\alpha^\beta}{\partial \boldsymbol{v}_0}\right)\Bigg|_{\boldsymbol{v}_0=\overline{\boldsymbol{v}_0^*}} \left(\frac{\partial T_\beta^\alpha}{\partial \boldsymbol{v}_1}\frac{\partial T_\alpha^\beta}{\partial \boldsymbol{v}_0}\right)\Bigg|_{\boldsymbol{v}_0=\overline{\boldsymbol{v}_1^*}} \frac{\partial p}{\partial \boldsymbol{x}_0}, \end{aligned}$$

respectively. We also observe a quite different construction in the corresponding matrices. Therefore, it is expected that the eigenvalues and eigenvectors of $\boldsymbol{x}_1^*$ and $\overline{\boldsymbol{x}_1^*}$ are dissimilar.

5. Conclusion

In this study, we investigated the structurally unstable synchronization phenomenon observed in the two-coupled Izhikevich neuron model. To analyze this phenomenon, we derived a discrete-time dynamical system that is equivalent to the original system. We established that the synchronous firing in the continuous-time dynamical system is equivalent to the border-collision bifurcation in the discrete-time system. Furthermore, we proposed an objective function that yields the parameter set at which the border-collision bifurcation arises. The function is numerically differentiable and can be solved using Newton's method. We have suggested some numerical techniques to obtain the Jacobian matrices with respect to the initial state and some parameter, λ. We have numerically obtained a bifurcation diagram in the (a_α, δ)-plane, which include the border-collision bifurcation sets. In the bifurcation diagram, we observed that the border-collision bifurcation sets construct a novel bifurcation structure that resembles the 'strike-slip fault' in geology. This structure implies that, before and after the border-collision bifurcation occurs, the stability of the periodic point discontinuously changes in some cases but maintains in other cases. Based on observations of the one-parameter bifurcation diagram and the collection of attractors, we have carefully confirmed the transition of the attractors through the bifurcations. In addition, we demonstrated that a border-collision bifurcation sets branch at distinct points. This results in the border-collision bifurcation diagram having a tree-like apperance; we refer to this structure as a border-collision bifurcation tree (BC tree). By further investigating the border-collision bifurcations, we observed discontinuous changes in the eigenvalues and eigenvectors of the periodic points and demonstrated that there exist two topologically different periodic points near the bifurcation. We provided evidence demonstrating that the periodic points that share a coordinate are topologically different near the border-collision bifurcation. We observed that in the discrete-time dynamical system, at the border-collision bifurcation, as one periodic point disappears, another one simultaneously appears, which corresponds to the change in the firing order in the continuous-time dynamical system.

In the future, synchronous firing phenomena in multiple coupled models should be investigated. It is expected that the objective function presented here can be naturally extended to the case of multiple coupled models. It is also of interest to investigate the case of chemical coupling as well as the electric coupling investigated here. The method presented here is likely to be capable of investigating such systems if discrete-time dynamical systems with a differentiable maps can be obtained for these problems. It is also of interest to consider the effect of a border-collision bifurcation in the global state space. In the Poincaré maps that include many unstable periodic points in the state space, the border-collision bifurcation is likely to significantly impact the periodic points and their stability. Observing the basin of attraction before and after the bifurcation would also be of interest. We conclude by noting that there remain a wide range of phenomena to be investigated in the two-coupled Izhikevich neuron model.

6. Acknowledgments

This work was partially supported by JSPS KAKENHI Grant Number JP23K13353 and JP21K04109.

References

Banerjee, S. & Grebogi, C. [1999] "Border collision bifurcations in two-dimensional piecewise smooth maps," *Physical Review E* **59**, 4052.

Chossat, P. & Lauterbach, R. [2000] *Methods in equivariant bifurcations and dynamical systems*, Vol. 15 (World Scientific Publishing Company).

Elkaranshawy, H. A., Aboukelila, N. M. & Elabsy, H. M. [2021] "Suppressing the spiking of a synchronized array of Izhikevich neurons," *Nonlinear Dynamics* **104**, 2653–2670.

Feudel, U., Neiman, A., Pei, X., Wojtenek, W., Braun, H., Huber, M. & Moss, F. [2000] "Homoclinic bifurcation in a Hodgkin–Huxley model of thermally sensitive neurons," *Chaos: An Interdisciplinary Journal of Nonlinear Science* **10**, 231–239.

Heidarpur, M., Ahmadi, A., Ahmadi, M. & Azghadi, M. R. [2019] "CORDIC-SNN: On-FPGA STDP learning with izhikevich neurons," *IEEE Transactions on Circuits and Systems I: Regular Papers* **66**, 2651–2661.

Hodgkin, A. L. & Huxley, A. F. [1952] "A quantitative description of membrane current and its application to conduction and excitation in nerve," *The Journal of Physiology* **117**, 500.

Ito, D., Ueta, T. & Aihara, K. [2010] "Bifurcation analysis of two coupled Izhikevich oscillators," *IEICE Proceedings Series* **44**.

Izhikevich, E. M. [2003] "Simple model of spiking neurons," *IEEE Transactions on Neural Networks* **14**, 1569–1572.

Kang, S. M., Choi, D., Eshraghian, J. K., Zhou, P., Kim, J., Kong, B.-S., Zhu, X., Demirkol, A. S., Ascoli, A., Tetzlaff, R. *et al.* [2021] "How to build a memristive integrate-and-fire model for spiking neuronal signal generation," *IEEE Transactions on Circuits and Systems I: Regular Papers* **68**, 4837–4850.

Kousaka, T., Ueta, T. & Kawakami, H. [1999] "Bifurcation of switched nonlinear dynamical systems," *IEEE Transactions on Circuits and Systems II: Analog and Digital Signal Processing* **46**, 878–885.

Kousaka, T., Ueta, T., Tahara, S., Kawakami, H. & Abe, M. [2002] "Implementation and analysis of a simple circuit causing border-collision bifurcation," *IEEJ Transactions on Electronics, Information and Systems* **122**, 1908–1916.

Lapicque, L. [1907] "Recherches quantitatives sur l'excitation electrique des nerfs traitee comme une polarization," *Journal de Physiologie et de pathologie générale* **9**, 620–635.

Ma, Y., Kawakami, H. & Tse, C. K. [2004] "Analysis of bifurcation in switched dynamical systems with periodically moving borders: application to power converters," *2004 IEEE International Symposium on Circuits and Systems (ISCAS)* (IEEE), pp. IV–701.

Miino, Y., Ito, D. & Ueta, T. [2015] "A computation method for non-autonomous systems with discontinuous characteristics," *Chaos, Solitons & Fractals* **77**, 277–285.

Miino, Y. & Ueta, T. [2016] "Synchronized firing phenomena and bifurcation in coupled Izhikevich neuron model," *IEICE Technical Report; IEICE Tech. Rep.* **116**, 51–56.

Nusse, H. E., Ott, E. & Yorke, J. A. [1994] "Border-collision bifurcations: An explanation for observed bifurcation phenomena," *Physical Review E* **49**, 1073.

Rozenberg, M., Schneegans, O. & Stoliar, P. [2019] "An ultra-compact leaky-integrate-and-fire model for building spiking neural networks," *Scientific Reports* **9**, 11123.

Sapounaki, M. & Kakarountas, A. [2019] "A high-performance neuron for artificial neural network based on Izhikevich model," *2019 29th International Symposium on Power and Timing Modeling, Optimization and Simulation (PATMOS)* (IEEE), pp. 29–34.

Shafiei, M., Parastesh, F., Jalili, M., Jafari, S., Perc, M. & Slavinec, M. [2019] "Effects of partial time delays on synchronization patterns in Izhikevich neuronal networks," *The European Physical Journal B* **92**, 1–7.

Simpson, D. J. [2016] "Border-collision bifurcations in r^n," *SIAM REVIEW* **58**, 177–226.

Tamura, A., Ueta, T. & Tsuji, S. [2009] "Bifurcation analysis of Izhikevich neuron model," *Dynamics of continuous, discrete and impulsive systems, Series A: mathematical analysis* **16**, 759–775.

Tolba, M. F., Elsafty, A. H., Armanyos, M., Said, L. A., Madian, A. H. & Radwan, A. G. [2019] "Synchronization and FPGA realization of fractional-order Izhikevich neuron model," *Microelectronics Journal* **89**, 56–69.

Vazquez, R. [2010] "Izhikevich neuron model and its application in pattern recognition," *Australian Journal of Intelligent Information Processing Systems* **11**, 35–40.

Vivekanandhan, G., Hamarash, I. I., Ali Ali, A. M., He, S. & Sun, K. [2022] "Firing patterns of Izhikevich neuron model under electric field and its synchronization patterns," *The European Physical Journal Special Topics* , 1–7.

Wang, G., Yang, L., Zhan, X., Li, A. & Jia, Y. [2022] "Chaotic resonance in Izhikevich neural network motifs under electromagnetic induction," *Nonlinear Dynamics* **107**, 3945–3962.

Yamashita, Y. & Torikai, H. [2012] "Bifurcation analysis of inhibitory responses of a PWC spiking neuron model," *Nonlinear Theory and Its Applications, IEICE* **3**, 557–572.